Protein Expression and Purification 236 (2025) 106808

Contents lists available at ScienceDirect

Protein Expression and Purification

journal homepage: www.elsevier.com/locate/yprep

Research Article

Advancing recombinant antibody production in *E. coli*: Optimization of expression and purification via dual GFP promoter and imaging technology

Anttoni Korkiakoski, Sami Oksanen, Tuomas Huovinen *

University of Turku, Department of Life Technologies, Turku, Finland

ARTICLE INFO

Keywords:
GFP
ONLINE SENSOR
BIOREACTOR
Recombinant ANTIBODY
FED-BATCH
E. COLI

ABSTRACT

Fed-batch fermentation results in high recombinant protein titers in limited culture volumes. Therefore, it is the preferred operation mode in the bioprocess industry. Optimizing feeding, induction, and harvest timing is a significant time-consuming challenge in bioprocessing complicated by the fact that expressed target protein is rarely detectable in real-time. In this study, the construction of an online sensor is described integrating a dual GFP promoter construct, a blue LED and a Raspberry Pi camera for real-time monitoring of recombinant antibody expression in *Escherichia coli*. The dual promoter construct allows simultaneous expression of GFP in the cytoplasm and the recombinant antibody in the periplasm, enabling the use of GFP fluorescence as a proxy for protein yield. GFP fluorescence correlated with Fab and nanobody expression over time and the relative quantity of fluorescence predicted the extent of induction. In nanobody fed-batch fermentations, the decreasing rate of dGFP/dt was a valuable parameter for identifying the optimal harvest point, minimizing excessive incubation time and reducing nanobody leakage into the medium. It was further demonstrated that quantitation of pixel values from RGB images captured with a Raspberry Pi 8 MP camera in the flow cell resulted in equal sensitivity for GFP detection as that achieved with a μPMT and photodiode sensors. The 3D-printable GFP sensor station is a valuable tool for process optimization and for educating bioprocess engineering students through real-time visualization of promoter activation.

1. Introduction

Antibody fragments, i.e., single-chain variable fragments (scFv), antigen-binding fragments (Fab), and single-domain antibodies such as nanobodies are a growing class of biomolecules with applications in pharmaceuticals, diagnostics and molecular imaging [1]. A scFv consists of the variable domains of the immunoglobulin light chain (VL) and heavy chain (VH) joined by a flexible linker; a Fab is a heterodimer composed of the light chain and the VH–CH1 domains of the heavy chain; whereas a nanobody is the variable domain of heavy-chain-only antibodies that naturally occur in camelids and is solely responsible for antigen recognition [2]. In contrast to full-length antibodies (~150 kDa), ScFvs, Fabs, and nanobodies with approximate molecular sizes of 27, 50, and 15 kDa, respectively, can be readily produced in cost-effective microbial systems [3].

Both intracellular and extracellular expression (ESETEC) and purification workflows have been established using *E. coli* as the expression host [4], but directing the antibody fragments to the periplasm with N-terminal secretory signal sequence is the most straightforward strategy for obtaining soluble and functional molecules [5]. The oxidative environment of the periplasm supports correct disulfide bond formation [6,7], whereas in the reducing cytoplasmic environment antibodies tend to express into inclusion bodies (IB) [4]. In addition to impaired disulfide bond formation, excess protein production can cause the accumulation of partially folded, aggregating intermediates in the cytoplasm, which can be alleviated by reducing induction and lowering temperature [8]. The advantage of inclusion bodies is that the target protein is fairly pure after extraction, denaturation and refolding process, but as the refolding process is time-consuming and challenging, expression directly into soluble format is typically desired [4].

Several analytical techniques, such as SDS-PAGE analysis, western blotting and microtiter plate immunoassays, are routinely used to monitor antibody expression [9]. These techniques are typically implemented after the expression experiment and require continuous manual sampling of the expression culture. As an alternative method, fluorescent proteins (FPs) have been linked to protein expression as fluorescence signal can be detected with an automated optical online sensor [10]. Green fluorescent protein (GFP) from the jellyfish *Aequorea*

* Corresponding author. Department of Life Technologies, University of Turku, Medisiina D6/ Room D6024, Kiinamyllynkatu 10, 20520, Turku, Finland.
E-mail address: tuohuo@utu.fi (T. Huovinen).

https://doi.org/10.1016/j.pep.2025.106808
Received 23 May 2025; Received in revised form 22 August 2025; Accepted 27 August 2025
Available online 28 August 2025

Victoria [11], and mutated derivatives thereof [12], have been used as a reporter for target protein expression directly and indirectly [13]. In the direct approach the gene coding for FP is genetically fused to the gene coding for the target protein and, consequently, increased fluorescence inherently correlates with increased protein yield [14]. In the fusion protein strategy, however, the GFP moiety must be cleaved off to gain the target protein in its native state [15]. Naturally, GFP fusion proteins as fluorescent molecules have many exploitable applications and their production is a viable concept in *E. coli* if GFP is allowed to fold in the cytosol [16]. In contrast, expression of antibodies as GFP fusions is not an option as GFP folds in the reducing environment of the cytoplasm [17], whereas antibodies are secreted and fold most effectively in the oxidative environment of the periplasm.

FPs can be used as indirect reporters for target protein expression by incorporating the FP gene into a bicistronic promoter construct, where both the gene of interest and the FP have their own ribosome binding sites, thereby avoiding problems associated with fusion proteins. In an early example by Daabrowski et al. (1999) the expression of proinsulin to inclusion bodies was monitored with a bicistronic construct containing YFP gene as a reporter [18]. It was observed that YFP fluorescence correlated with proinsulin expression during the bioprocess, and fluorescence could, therefore, be used as a surrogate for target protein expression. Alternatively, dual promoter constructs have been created. Recently, Tan et al. (2020) generated a dual promoter system for the simultaneous expression of 5-ALA synthetase and superfolder GFP (sfGFP) demonstrating that also in dual promoter configuration fluorescence signal correlated with the target product yield [19]. In these examples FP monitoring was performed off-line with a microplate reader.

Data on protein expression dynamics over time from production experiments is a valuable tool for process optimization. There are three prior reports on applying an online GFP sensor for high cell density fermentation, of which, in the earliest example an LED was used for FP excitation and a photomultiplier tube (PMT) for capturing the emitted light [20]. In an upgraded version from the same laboratory the cumbersome and expensive photomultiplier tube was replaced with a photodiode [21]. In the third report by Jones et al. (2004) a readily available commercial fiber optic online spectrophotometer was used for monitoring GFP containing an LED for excitation and a linear CCD array for detection [14]. This study demonstrated the advantages of in-situ fluorescence monitoring compared to conventional production without real time monitoring, as product yield was found to be pH dependent, allowing corrective pH adjustments during fermentation to maximize yield. In addition, online sensing revealed that the target protein was expressed for a longer period than previously expected, providing valuable information for optimizing batch yield.

Performance of digital cameras has greatly improved over the years and integrated cameras of smart phones have been considered as reliable instruments for fluorescence microscopy [22], bioluminescence detection [23] and fluorescence-based diagnostics [24]. In the study by Aufdembrink et al. (2020) a single board Raspberry Pi computer was used with a cell phone camera module, which is the most versatile solution of the three as the image capture and analysis can be automated with simple Python code run on the single board computer [24]. Currently, the price for the smallest application-ready microspectrophotometer for fluorescence detection is $>$ 1000 € (October 2024, https://www.oceaninsight.com), whereas a Raspberry Pi computer along with the Raspberry Pi 8 MP camera module can be purchased with ~100 € [25].

Although online GFP sensors have been developed for process monitoring, published studies have applied the technology only to real-time detection of fluorescent proteins or reporter–target protein fusions [14,20,21]. In contrast, studies introducing the more relevant bicistronic or dual-promoter fluorescent constructs have measured fluorescence offline using plate readers [18,19]. Combining a dual-promoter system with online detection would uniquely enable real-time tracking of recombinant protein expression, thereby facilitating process optimization while allowing downstream purification of the target protein in its native state.

In this study, we present a modular dual-GFP promoter plasmid for real-time monitoring of protein expression in *E. coli* cultures. We demonstrate that the rate of GFP fluorescence accumulation reliably reflects not only cytoplasmic protein yield, as previously reported [18,19], but also periplasmic expression levels of recombinant targets. In addition, we developed a low-cost online GFP sensor using blue LED excitation and a Raspberry Pi 8 MP camera for detection, providing sensitivity comparable to that of conventional plate readers. This tool proved particularly effective for assessing induction efficiency and determining the optimal harvest time for Fab fragment and nanobody production in *E. coli* fermentations.

2. Materials and methods

2.1. DNA constructs and small-scale protein expression

The variable domain sequences of Fab CR3009 were obtained from the study by van den Brink et al. [26] and designed as a fusion with in-house human CH1 and kappa constant domain DNA sequences creating a Fab fragment (amino acid sequence provided in supplementary material). The Fab cassette with flanking SfiI sites was ordered from Twist Bioscience (USA) and ligated with SfiI to pLK06H vector [27] according to standard cloning procedures. Minipreps were prepared from selected clones (GeneJET miniprep kit, Thermo Scientific, USA) and a clone with correct DNA sequence according to DNA sequencing results (Macrogen, South-Korea) was taken for continuation.

LacP/O-GFP cassette was ordered as synthetic DNA with flanking HindIII R.E. sites (DNA sequence provided in supplementary material) from Twist Bioscience (USA) and inserted into the HindIII site of pLK06H-Fab CR3009 vector, which was readily linearized with HindIII and dephosphorylated with FASTAP (Thermo Scientific, USA) to avoid self-ligation, according to standard cloning procedures. The GFP variant used in the study is wild-type GFP (avGFP) with the mutations F64L, S65T, Q80R, M153T and V163A, which improve GFP brightness, solubility, stability, folding efficiency, and cause a red-shift in the excitation peak, thereby improving compatibility with the standard fluorescein filter set for fluorescence detection [28,29]. The variant is similar to folding reporter GFP without F99S mutation [30]. Minipreps were prepared and clones sequenced as above. Two plasmids were selected for expression termed pLK06Hpp-Fab clone 1 (Addgene plasmid #239861) and 2, containing GFP cassette in opposite direction, respectively.

The sequence of the anti-human IgG CH1 nanobody expressed in fed-batch experiments was retrieved from literature [31] synthesized by Twist biosciences and cloned with SfiI restriction sites into pAK400 [32] that is routinely used for periplasmic expression in our laboratory. The Nanobody gene was further modified with K84H mutation (termed Nb) and by adding three lysines at the C-terminal end preceding the Histag (termed Nb3K). Nb and Nb3K sequences are provided in the supplementary file. pAK400pp was constructed similarly to pLK06Hpp by inserting LacP/O-GFP cassette HindIII-cassette to the HindIII site of pAK400 vector. Mutant Nb genes were cloned with SfiI into pAK400pp vector, verified by Sanger sequencing (Macrogen Inc) and transformed to BL21 for expression experiments. Vector map (Fig. S1) and the nanobody sequences are in the supplementary material.

E. coli XL-1 Blue (Agilent, USA) harbouring pLK06Hpp-Fab CR3009 clones 1 and 2 were precultured overnight in 5 ml of SB medium containing 1 % w/v glucose (glc) and 100 μg/ml ampicillin (amp) at 37 °C with 300 rpm shaking. SB medium contains 30 g/L tryptone, 20 g/L yeast extract and 10 g/L MOPS in pH 7.0. The clones were expressed in 5 ml SB (0.05 % w/v glc and 100 μg/ml amp) by inoculating precultures to OD 0.05 and incubating cultures at 37 °C with 300 rpm shaking. At OD 0.6–0.8 the cultures were induced with 0 μM, 10 μM or 200 μM IPTG and

incubation continued overnight at 26 °C with 300 rpm shaking. The cells were harvested by centrifugation (3220 g for 10 min at 4 °C) and the pellets resuspended in 1 ml lysis buffer containing 1 mg/ml lysozyme (Alfa Aesar, USA) and 25 U/ml Pierce Universal Nuclease (Thermo Scientific, USA) in PBS pH 7.4. For lysis, the cell suspensions were incubated for 30 min at room temperature on rotation after which the suspension was freeze-thawed three times. The cell debris was pelleted by centrifugation (16 100 g for 10 min at 4 °C) and the resulting supernatant was used for the assay. The protein expression experiment was repeated three times on separate days. The experiment to study the effect of GFP co-expression on Fab–alkaline phosphatase (Fab–AP) yield was performed as above using 200 μM IPTG for induction.

2.2. Time course analysis

XL-1 Blue with pLK06Hpp-Fab CR3009 clone 1 was grown as above except that for 100 ml cultures in 500 ml shake flasks (250 rpm, induction with 200 μM IPTG) were used for protein expression phase. To follow the GFP and Fab-AP expression, 2 ml samples were taken from the flask every hour starting at induction for a 10 h time period. Turbidity of the samples was measured directly after withdrawal at 600 nm with spectrophotometer (Shimadzu, Japan) from appropriate dilution. Furthermore, GFP and Fab-AP measurements were carried out as described below.

2.3. Analysis of GFP and Fab-AP concentrations

GFP fluorescence was measured from 1:100 dilutions in PBS on clear C12 Maxisorp well strips (200 μl/well, Thermo Scientific) with Hidex Sense-plate reader (Hidex, Finland; using 485 nm for excitation with 10 nm bandpass and 535 nm for emission with 20 nm band pass). The fluorescence values were converted to concentrations based on the fluorescence curve obtained from GFP standard dilution series (5 μM–78.125 nM). Fab-AP concentrations were determined based on alkaline phosphatase activity of the fusion from 1:1000 dilutions in pNpp buffer (1 mg/ml p-nitrophenyl phosphate (Sigma-Aldrich, USA), 500 mM Tris-Cl pH 9.0, 200 mM NaCl and 10 mM $MgCl_2$). The samples were incubated in 200 μl/well volume on clear C12 Maxisorp well strips for 1 h at room temperature with low shaking and absorbance at 405 nm was read using Victor 1420 Multilabel Counter (Wallac, Finland). All measurements were performed using triplicate wells.

2.4. Measurement unit and data processing

The circuit diagrams for photodiode and μPMT control are in supplementary data (Fig. S2 and S3). 8 MP Raspberry Pi Camera Module v2 (Raspberry Pi Foundation, United Kingdom) was used for the detection of GFP fluorescence. The camera was mounted in the camera port of Raspberry Pi 4 Model B 2 GB (Raspberry Pi Foundation) according to manufacturer's instructions. A blue 5 mm LED (LED 5SUK12V, Elgood Oy, Finland) with a built-in resistor and a peak intensity at wavelength of 467 nm was used as the excitation source of the measuring device. The LED was attached to a watertight metal holder containing a lens (SML1083, Signal Construct, Germany) with a focal length of 15 mm. The excitation light was filtered with a 470-nm band-pass filter (FB470-10, Thorlabs, Germany) and the emitted light from the glass cylinder (Pasteur pipette) was filtered with a 510-nm band-pass filter (FB510-10, Thorlabs). The bandwidth of both filters was 10 nm. The spectra of the LED, bandpass filters and GFP (University of Turku, Finland) were measured with an Ocean Optics (USA) HR-4000-UV-NIR spectrophotometer (Fig. S4). Explosion views for assembling the camera and LED modules are in Fig. S5.

The LED and sensors were housed inside 3D-printed modules with adjustable angles for the alignment of excitation and emission light paths (Fig. S6). The modules were installed inside a 3D-printed box consisting of two parts for easy installation of the sterilized flow cell (Pasteur pipette) and silicon tubing. AutoCAD and Tinkercad (Autodesk Inc, USA) were used for designing the GFP measuring station. All parts were printed with 1.75 mm polylactide filament (Prusament PLA, Prusa Polymers, Czech Republic) and 0.4 mm nozzle on PEI-coated metal sheet with either i3 MK3S-3D or MK4 printer (Prusa Research, Czech Republic) using standard settings recommended by the manufacturer. The two largest prints required applying glue stick on the PEI sheet to avoid warping at the far-edges of the printing area. M4 bolts and nuts were used in the construction of the measuring station and modules. The 3D files and assembly component list are available on GitHub (https://github.com/tuohuo/gfpsensor).

In the first embodiment, for comparing the light detection sensors, Arduino Uno Rev3 microcontroller was used to control the LED with an N-channel MOSFET (IRFZ44N, International Rectifier, USA). To this end, the output analog signal V_{out} of the amplifier circuit was converted to a digital signal by an ADS1115 A/D converter (Adafruit, USA), which in turn was connected to the microcontroller via an I2C interface. This arrangement supported pulse width modulation allowing the adjustment of the brightness of the LED. For all further experiments, the circuit was simplified by connecting the LED to S8050 NPN bipolar junction transistor (BJT) powered with 5V output from the Raspberry Pi and controlled with GPIO18 pin (base), which also supports pulse-width modulation. The LED intensity was, however, kept at the maximum throughout the experiments. The circuit diagram for LED control is described in Fig. S7.

For detection sensor comparison, the fluorescence signal was converted to digital form with photodiode and μPMT as described in supplementary materials. For detection with camera, a Python script was used to capture images with 1600 x 1200 width-height resolution with 1 s exposure time and ISO800 value. The images were saved as.jpg-files, converted to grey scale and all pixel values were summed to obtain a value for the fluorescence signal. In camera experiments without band pass filters only the sum of green pixel values was taken as the fluorescence intensity value. Both excitation and emission band pass filters were in place for monitoring batch and fed-batch fermentation experiments. Python script for controlling the Raspberry Pi camera and LED is provided in the supplementary materials. For detection sensor comparison, a serial 1:1 dilution of GFP (10 μM–0.6 nM) was prepared in PBS.

2.5. Batch experiments in bioreactor

The effect of IPTG induction on Fab-AP expression and GFP fluorescence was studied by batch fermentation experiments in *E. coli* BL21 strain with pLK06Hpp-Fab CR3009 clone 1 in 5 L KLF stirred-tank bioreactor (Bioengineering AG, Switzerland). The GFP-free control experiment was performed with pLK06H-Fab CR3009 plasmid lacking the GFP-cassette. Overnight preculture was diluted to OD600-value of 0.05 in 3.4 L SB main culture supplemented with 100 μg/ml carbenicillin and 0.05 % w/v glucose. The culture was aerated with 300 L/h air with 500 rpm stirring at 30 °C. Ten drops of Sigma Antifoam 204 (Sigma-Aldrich) was added at the beginning of the fermentation. Dissolved oxygen concentration was kept at min 30 % with a cascade control by adjusting stirrer speed and air rate. The cascade control was activated when pO_2 decreased below 35 %. In the induced batches, IPTG was added to 400 μM final concentration at OD600 0.8. The GFP online sensor was connected to the drain port of KLF reactor and to the lid of the reactor with a 1.6 m silicone tubing with i.d. 3 mm and o.d. 6 mm (Novosil, Fisher scientific). The flow was controlled with KLF peristaltic pump (5 s pulse width and 10 % duty cycle). 10 cm peristaltic pump-compatible PharMed BPT tubing (Saint-Gobain, i.d. 3.2 mm and o.d. 6.3 mm) was connected to the line with male and female luer lock connectors (luer with lock ring for 3.2 mm i.d. tubing, nylon, MasterFlex). Images were captured every 5 min with the settings described above and processed with a Python script provided in the supplementary material to plot separately the pixel-sum values of green, red and blue

channels in real time. Fab-AP expression was followed with a pNpp colorimetric assay as described above.

2.6. Fed-batch experiments in KLF

Semi-synthetic batch medium (3 L) was similar to Ref. [29] and consisted of 7 g/L KH_2PO_4, 0.26 g/L K_2HPO4, 10.5 g/L $(NH_4)_2SO_4$, 1.26 g/L NaCl, 1.16 g/L K_2SO_4, 0.014 g/L $CaCl_2{\cdot}2H_2O$, 0.15 g/L $MgSO_4{\cdot}7H_2O$, 0.53 g/L yeast extract, 10 g/L glucose and 0.125 mL/L trace element solution. pH was adjusted to 7.0 with NaOH. Trace element solution was dissolved in 5 N HCl and consisted of 40 g/L $FeSO_4{\cdot}7H_2O$, 10 g/L $MnSO_4{\cdot}H_2O$, 4 g/L $CoCl_2$, 2 g/L $ZnSO_4{\cdot}7H_2O$, 2 g/L $Na_2MoO_2{\cdot}2H_2O$ and 0.5 g/L H_3BO_3. The feed medium (1 L) consisted of 100 g/L glucose, 1.5 g/L $MgSO_4{\cdot}7H_2O$, 27.5 g/L $(NH_4)_2SO_4$, 0.026 g/L $CaCl_2{\cdot}2H_2O$ and 2.5 mL/L trace element solution. The fed-batch experiments were performed in 5 L KLF stirred-tank bioreactor using *E. coli* BL21 as the host strain. During fermentation, pH (set point at pH 7) and foaming were controlled with a closed feed-back loop with 20 % ammonia and Sigma 204 antifoam (Sigma-Aldrich), respectively. Aeration was controlled with a cascade control as described above. The reactor was inoculated with a preculture to initial OD600-value of 0.05 and incubated at 30 °C. When glucose was consumed in the batch fermentation indicated by the increase of D.O. over 50 % saturation, feed-phase was started. Feeding followed an exponential feeding profile with equation (eq (1)):

$$F = F_0 * e^{\mu t} \quad \text{(eq1)}$$

where μ is the desired growth rate, which was set to 0.15 h^{-1}, t is time and F_0 is the initial feeding rate. Initial feeding rate was calculated with formula (eq (2)):

$$F_0 = \frac{(\mu/Y_{em} + q_m)*(XV)}{S_{in}} \quad \text{(eq2)}$$

where μ is the set desired growth rate, Y_{em} is the yield coefficient exclusive maintenance (0.5 $g_{biomass}/g_{glc}$), q_m is the maintenance coefficient (0.025 $g_{glc}/(g_{biomass}h)$), S_{in} is the glucose concentration (100 g/L) in the feed medium, XV is the product of cell concentration (g/L) and volume (L) at the end of the batch phase. In Nb3K fermentation at 24h harvest time point, half of the medium was withdrawn from the reactor and feed medium was replaced with ½ diluted fresh (1 L) solution to keep the glucose feeding rate unchanged in relation to generated cell mass.

2.7. Downstream processing of harvested cells

At Nb and Nb3K fermentation harvest time points, cells were collected on ice-water bath from the bottom valve and cells were pelleted for 10 min at 6000 rpm at 4 °C using JA-10 rotor (Avanti J-26XP centrifuge, Beckmann-Coulter). In Nb purification, medium was fractionated by $(NH_4)_2SO_4$ precipitation at increasing concentrations. First, the medium was supplemented to final 51 % ammonium sulfate concentration and incubated overnight at 4 °C with magnet stirrer and centrifuged 30 min at 10 000 rpm at 4 °C (JA-10). Supernatant was decanted and supplemented with $(NH_4)_2SO_4$ to final 57 % concentration and incubated 4 h at 4 °C. The precipitate was pelleted as above and resulting supernatant reprecipitated at final 70 % $(NH_4)_2SO_4$ concentration overnight at 4 °C.

Nb cell pellet was resuspended in 1 L TBS pH 7.4 containing 1 mg/ml lysozyme (Sigma-Aldrich), 1:50 000 diluted Pierce Universal Nuclease (Thermo Fisher Scientific) and 1 mM $MgCl_2$. The cell suspension was incubated for 30 min at RT with gentle rocking and passed through three freeze-thaw cycles. The resulting lysate was centrifuged for 30 min at *50 000 g* at 4 °C to pellet cell debris, after which, the supernatant (cleared cell lysate) was decanted and supplemented with $(NH_4)_2SO_4$ to final 80 % concentration. The precipitation was incubated overnight at 4 °C with stirring and centrifuged 30 min at 10 000 rpm at 4 °C (JA-10). Precipitated Nb pellets were resuspended in 200 ml PBS pH 7.4 supplemented with 10 mM imidazole and centrifuged for 30 min at *50 000 g* at 4 °C to pellet undissolved material. The supernatant was loaded on custom 5 ml NiNTA column packed with HisPur Ni-NTA resin pre-equilibriated with 10 mM imidazole in PBS. After sample loading, the column was washed 10x CV with 10 mM imidazole in PBS and bound proteins eluted with 300 mM imidazole in PBS pH 7.4. The flow rate was kept constant at 2.5 ml/min throughout the NiNTA purification. The NiNTA elution peak was collected and concentrated with Vivaspin Turbo 4 MWCO 3000 ultrafiltration devices (Thermo) to < 10 mL volume, centrifuged for 10 min at *20 000 g* at 4 °C and the resulting supernatant was filtered with 0.22 μm filter. Size exclusion chromatography was performed with HiLoad 26/60 Superdex200 column (Cytiva) using TSA (TBS + 0.02 % NaN_3, pH 7.5) as the running buffer at constant flow rate of 2.6 ml/min. The sample was injected on the column from 10 ml loop. All chromatography experiments in this study were performed on ÄKTA Pure 25M chromatography system (Cytiva) collecting 2 ml elution fractions on 2 ml deep well plates. NiNTA flow-through was collected and reloaded on re-equilibriated 5 ml NiNTA column and purified according to the method described above. The NiNTA-SEC purification was repeated also for the second NiNTA column flow-through sample. Schematic workflow of Nb purification is described in Fig. S8.

Nb3K cell pellet after 24h and 29h of fermentation were treated similarly. Due to lower obtained cell mass than in the Nb fermentation, the pellet was directly resuspended in 200 ml PBS pH 8.2 with 10 mM imidazole, 1 mg/ml lysozyme, 1:50 000 diluted Pierce Nuclease and 1 mM $MgCl_2$. After passing the cell sample through three freeze-thaw cycles, sequential NiNTA and SEC chromatographies were performed as described above. Due to higher pI value of Nb3K (7.25) compared to Nb (6.22), all NiNTA buffers were adjusted to pH 8.2 and TSA buffer to pH 8.3.

2.8. SDS-PAGE and western blotting

For analysing Nb3K sample series, 1 ml samples were taken from the reactor at indicated time points and immediately centrifuged for 5 min with *16 000 g* at 4 °C. The supernatant was transferred to a fresh tube and the pellet resuspended in 1 ml of fresh medium. The samples were frozen for analysis with western blotting. After de-freezing, cell pellet samples were diluted 1/5 for SDS-PAGE. 5 μL of samples were mixed with 5 μL of reduced Laemmli buffer (2x concentrate, Bio-Rad, USA) and heated for 5 min at 95 °C. The samples were run on 4–15 % SDS-PAGE (Bio-Rad, USA) at 200 V for 32 min and transferred with Trans-Blot Turbo semidry transfer cell (Bio-Rad, USA) on Ø 0.2 μm PVDF with settings: 2.5 A, 25 V, and 7 min transfer time. The PVDF membrane was blocked with 10 % fat-free milk (blotting grade blocker, BioRad, USA) in PBST0.05 (PBS + 0.05 % Tween-20) for 30 min at RT with rocking. The membrane was incubated with 1/2500 dilution of anti-His tag HRP antibody (HRP-66005, Proteintech Group, USA) in 10 % fat-free milk in PBST0.05 for 45 min. PVDF membrane was washed 3 × 5 min with PBST0.05, and Nb3Ks detected with precipitating TMB (Sigma-Aldrich, USA). All protein purification samples were run on SDS PAGE as described above and stained with InstantBlue (Sigma-Aldrich) according to manufacturer's recommendations.

3. Results

3.1. Protein expression using dual promoter GFP construct

The dual GFP reporter construct was studied by co-expressing GFP with a human Fab recognizing the nucleocapsid protein of SARS-COV coronaviruses. Although clone CR3009 was generated against SARS-COV-1, it is cross-reactive to nucleocapsid protein of SARS-COV-2 (data not shown) and, therefore, potential candidate for COVID-19 diagnostics. Expression vector pLK06H-Fab was used as the starting point

for the dual promoter cloning experiment. In this vector, the Fab is transcribed as bicistronic mRNA under Lac P/O, in which, the light chain and heavy chain are encoded with N-terminal PelB signal sequences for periplasmic secretion (Fig. 1). In addition, the heavy chain is fused to bacterial alkaline phosphatase (Fab-AP) via the C-terminus. The GFP reporter functionality was designed to be added with a universal method. Therefore, a block of DNA containing both Lac P/O and a GFP gene flanked by HindIII sites was inserted into a HindIII site of pLK06H-Fab vector located downstream from the antibody gene. As it is possible for the Lac P/O-GFP cassette to be ligated in two opposite orientations in the vector, we isolated both constructs to study the effect of the orientation of the co-expressed GFP cassette on the Fab yield and induction by IPTG. The final dual GFP reporter vector maps carrying CR3009 Fab-AP clone are shown in Fig. 1.

Using pLKO6Hpp-Fab vector, the amount of Fab-AP and GFP protein concentrations increased as a response to increasing IPTG concentration. There was a strong positive correlation between the amount of Fab expressed and GFP fluorescence (R^2: 0.992 and 0.961, n:3). Construct 1, in which the *Lac* promoters were transcribed to the same direction, yielded systematically 12 % more Fab-AP than construct 2 at the same inducer concentration (Fig. 2).

Two-tailed *t*-test was performed to analyse the significance of the difference in Fab-AP expression between constructs 1 and 2 at different induction levels. The difference was significant at the basal state (0 μM; $p = 0.03$) and at 200 μM IPTG ($p = 0.01$). At 10 μM IPTG, construct 1 produced more Fab-AP than construct 2 in line with the other measurement points, but the difference was not statistically significant ($p = 0.09$). Parallel shake flask experiments were carried out with and without the dual GFP promoter cassette to study if overexpression of GFP simultaneously with Fab-AP would have a negative impact on the total yield of Fab-AP. The co-expression of GFP did not have a negative effect on the total yield of Fab-AP (Fig. 3).

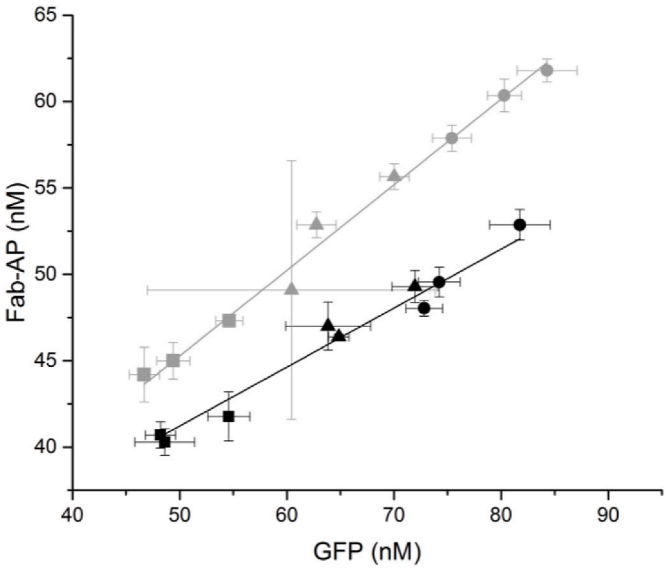

Fig. 2. The effect of orientation of the Lac P/O-GFP cassette on Fab-AP expression. Grey symbols: clone 1 in which the coding sequence of GFP gene and Fab genes are on the same DNA strand. Black symbols: clone 2 in which the coding sequence of GFP gene and Fab genes are on the opposite DNA strands. Protein production was induced with 0 μM (□), 10 μM (Δ) or 200 μM IPTG (○) as three replicates. The GFP fluorescence and Fab-AP concentration had a linear correlation. The fit function for clone 1 was $y = 0.495x + 20.5$ ($R^2 = 0.992$, grey line) and for clone 2, $y = 0.341x + 24.2$ ($R^2 = 0.961$, black line).

3.2. Design of measurement unit and comparison of the dynamic range and sensitivities of detection sensors

The GFP sensor unit for monitoring promoter activation was designed as a separate stand-alone instrument to which a continuous medium stream from the bioreactor was directed with a peristaltic pump (Fig. 4A). A glass Pasteur pipette made of durable borosilicate was used as an autoclavable flow-through chamber along with attached silicone tubing. As the fermentation broth in the bioreactor is intensively aerated, the bypass for the online GFP sensor station was attached to the bottom of the reactor withdrawing sample stream under the air sparger ring minimizing optical interference arising from air bubbles. The sample stream was returned to the bioreactor through a sterile needle port connection on the lid. The flow rate in the bypass was controlled by a peristaltic pump on the control tower of KLF bioreactor.

A blue led was chosen as the light source as it has a peak intensity at 467 nm, close to the GFP excitation maximum of 490 nm GFP (Fig. S4). Different light detection elements for the emitted light from GFP were compared to find the most robust, cost effective and sensitive solution for the task. A photodiode, a microphotomultiplier tube (μPMT) and a Raspberry Pi 8 MP camera were compared with identical excitation (460–480 nm band pass) and emission (500–520 nm band pass) filter sets. The light source and detector were aligned at an 85° angle for fluorescent light detection with adjustable screws (Fig. 4B).

The camera detected GFP with the same sensitivity as the μPMT, achieving a detection limit of 19.5 nM GFP in PBS (Fig. 5). Photodiode was less sensitive with a response range from 156.3 nM to 10 μM GFP. Furthermore, the sensor could be operated even in a simpler

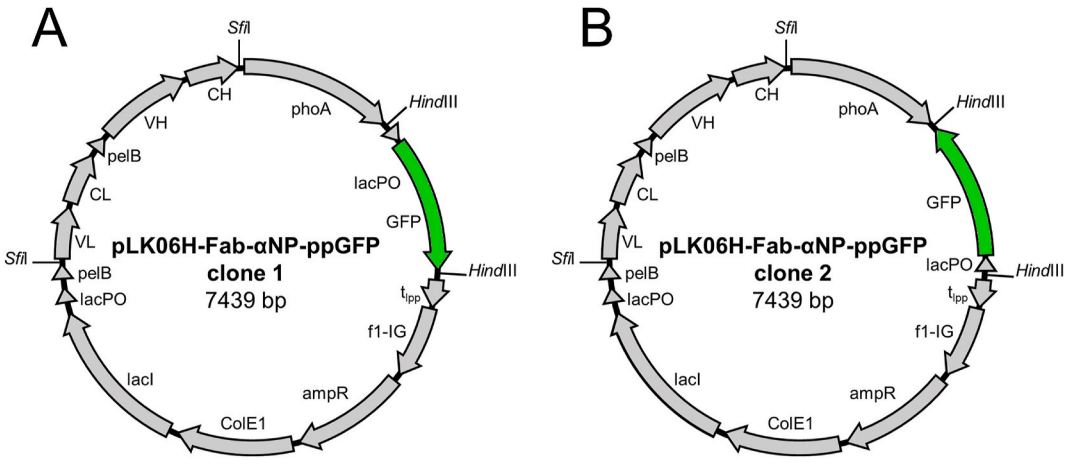

Fig. 1. Vector maps of dual GFP expression plasmids. A) In clone 1, the DNA cassette containing Lac P/O and GFP gene are in identical direction to the Fab gene cassette. B) In clone 2, the DNA cassette containing Lac P/O and GFP gene are in opposite direction to the Fab gene cassette.

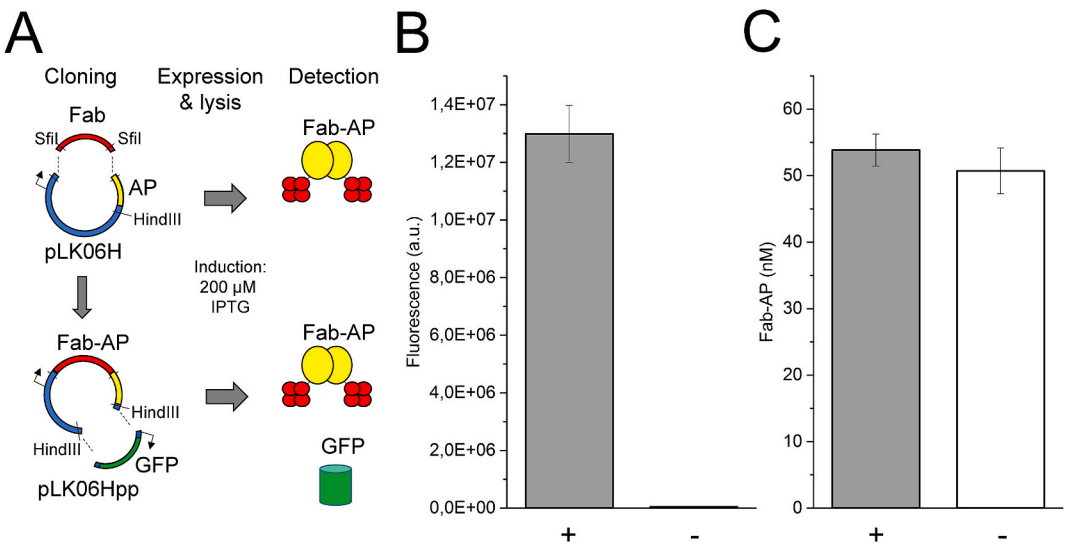

Fig. 3. The effect of GFP co-expression on the total yield of Fab-AP. (A) Cloning and expression workflow with expected outcome. Constructs pLK06Hpp-Fab clone 1 with dual GFP expression module (+) and pLK06H-Fab without GFP expression module (−) were expressed and analysed for GFP fluorescence (A) and Fab-AP concentrations (B). The error bar shows intra-assay variation of three replicate wells.

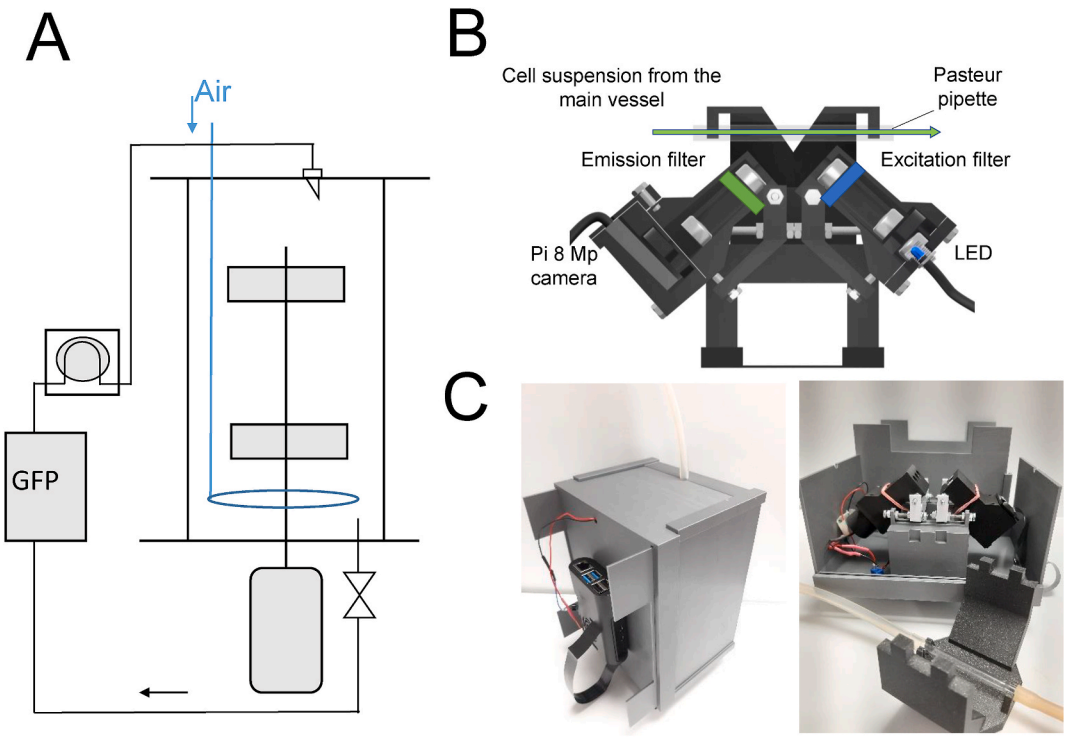

Fig. 4. Experimental setup for quasi-online GFP sensor. A) Side stream of 13.5 ml/min was pumped from the bioreactor via bottom drain valve to the sensor station and returned to the main vessel. B) Flow diagram of the measurement configuration and details of the culture flow-through the bubble trap unit. C) Online flow-through sensor station housing the camera.

configuration as the camera could be used as a GFP detector without band pass filters relying on the built-in Bayer color filter array for RGB color detection on the Raspberry Pi camera (Sony CMOS IMX219 Exmor sensor surface). For GFP measurement without band pass filters, only the sum of green pixel values was used, which resulted in a similar response curve comparable to the less sensitive photodiode. The unprocessed image series of GFP standard curve samples with emission and excitation filters in place is presented in Fig. 6. In the following experiments, the camera was chosen as the GFP detector because it demonstrated equal or higher sensitivity compared to other tested detectors while being simpler to install and more versatile to use.

With the implemented bypass stream circulation and the online sensor station design, the volume of culture medium outside the bioreactor was minimized. At any given time 25 ml of medium was outside the thermally controlled bioreactor, which is 1–0.6 % of the total working volume of 2.5–4 L and, therefore, does not have a significant effect on the growth dynamics of *E. coli* cultivated in the reactor. The delay time from vessel to sensor station was calculated with a spiked GFP pulse experiment (20 mL 10 µM GFP into 1980 mL PBS). Integrated Bioengineering KLF peristaltic pump was set to circulate medium stream

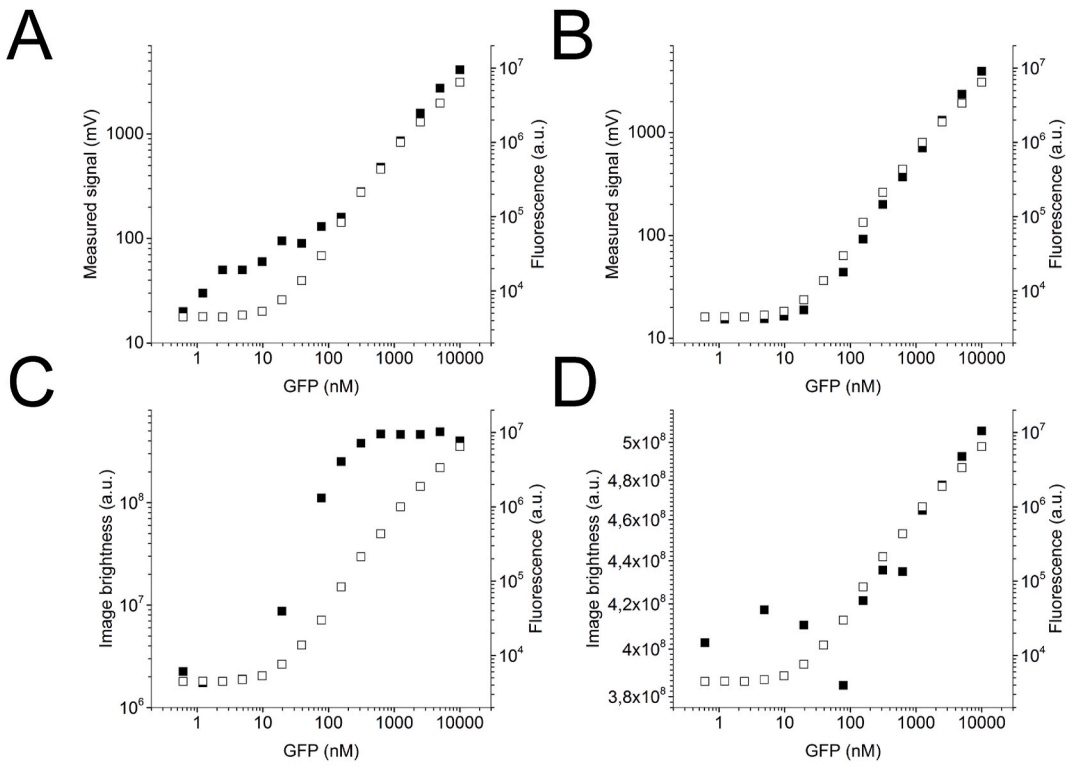

Fig. 5. Comparison of detection sensor performance for GFP fluorescence measurement. The reference curve (white squares) was measured with standard fluorescein filter set on Victor 1420 Multilabel Counter (Wallac, Finland). A) For photodiode, the dynamic range of response was from 156.3 nM to 10 μM GFP and B) for μPMT, from 19.5 nM to 10 μM GFP. The dynamic range of Raspberry Pi camera for GFP fluorescence detection was dependent on the use of excitation and emission filters. With excitation and emission filters in place (C) the dynamic range of response of the Raspberry Pi camera was from 19.5 nM to 312.5 nM and without filters (D) from 312.5 nM to 10 μM.

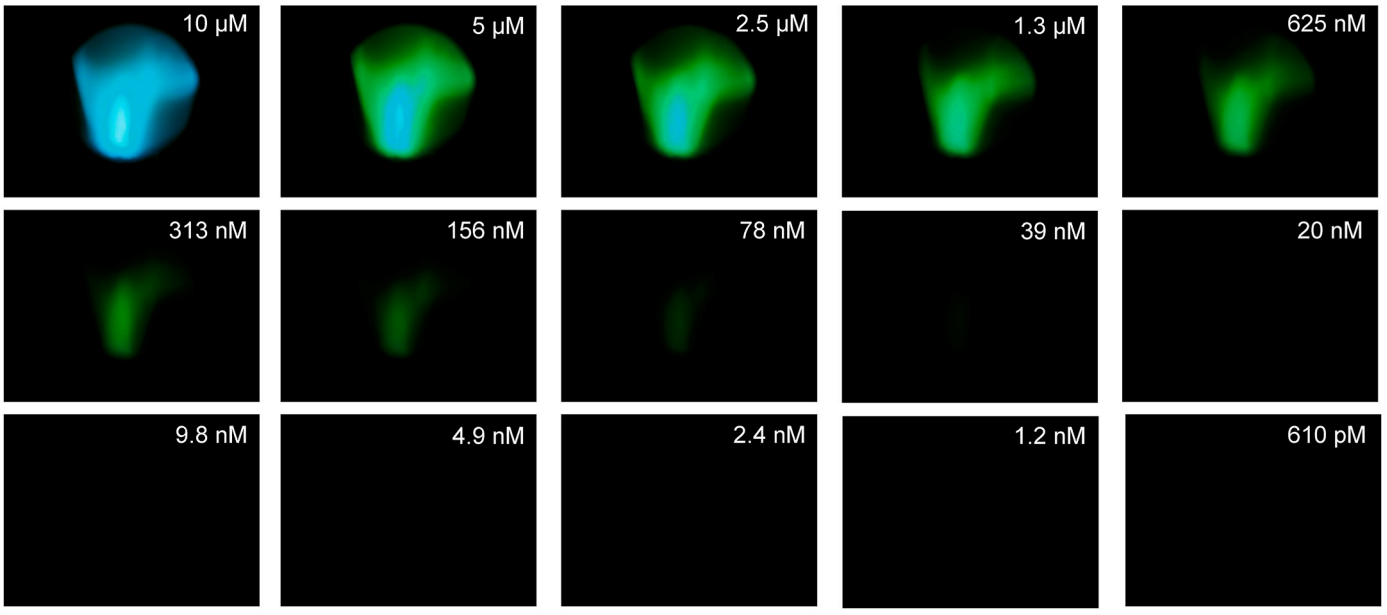

Fig. 6. Images of standard GFP concentrations in the flow cell (a Pasteur glass capillary). The cell was excited with blue led and images were taken with 8 MP Pi camera v2.1 with 1600x1200 width-height resolution using 470-nm and 510-nm band-pass filters (± 10 nm) for excitation and emission light, respectively. (For interpretation of the references to color in this figure legend, the reader is referred to the Web version of this article.)

at 5 s cycle time and 20 % duty cycle with 160 cm (3 mm I.D.) silicon tubing between the drain valve and GFP sensor cell. This flow rate was used as default for the GFP bypass stream during fermentation runs. In these conditions half maximal GFP saturation signal was obtained in 99 s from spiking. At 100 % duty cycle the half maximal fluorescence was obtained in only 24 s.

3.3. Monitoring batch fermentations for recombinant antibody production with GFP sensor

The usability of the online GFP sensor for following lac promoter activation was further studied in batch fermentations in 5 L Bioengineering KLF vessel, in which, CR3009 Fab-AP clone expression was induced with 400 μM IPTG and compared to non-induced condition. No GFP parallel promoter containing pLK06H-Fab CR3009 construct was used as control. The trace data shows nine-fold increase in GFP signal upon induction. In the absence of inducer 2.4-fold accumulation of GFP signal over the background was observed (Fig. 7A), which is in line with the well-known basal activity of lac promoter [33]. The GFP sensor signal does not increase over the time course in the induced control fermentation without the parallel GFP promoter. This verifies the autofluorescence arising from cell growth or other components in the medium does not cause interference in reading the induced GFP fluorescence from dual promoter constructs. The final cell turbidity values of the cultures measured after 17 h as OD600 values were 19.2, 16.4 and 12.8, for the parallel promoter construct with induction, without induction and with induction but without GFP, respectively. It was further confirmed with parallel promoter samples that the Fab-AP concentration correlated with the state of induction (Fig. 7B).

3.4. Monitoring of fed-batch fermentation for nanobody production with GFP sensor

We investigated the utility of the developed GFP reporter platform to inform on optimal harvest time in recombinant protein production processes by producing a nanobody in fed-batch fermentation. The chosen nanobody recognizes the CH1 domain of human IgG [31] and was cloned to pAK400pp vector to be expressed with a C-terminal histag. The clone was selected for production as it can be utilized as a capture or label reagent for human Fabs. The vector contains the GFP parallel promoter construct cloned in as HindIII cassette. Two variants of the nanobody sequence were expressed using BL21 as the host strain, of which, the other contained a K84H mutation (Nb) and the other three additional lysine residues between the histag and Nb-gene (Nb3K). The sequences are provided in the supplementary materials.

The fermentations were started with 3 L semi-synthetic medium in the batch phase containing 10 g/L glucose. After the glucose was consumed the batch was fed with a glucose feed solution following an exponential feeding profile to retain the specific growth rate μ at 0.15 h^{-1} assuming Y_{em} and q_m to be 0.5 g biomass/g glc and 0.025 g glc/(g biomass*h), respectively. A rising dissolved oxygen (D.O.) signal over 50 % saturation was used as the trigger for starting the medium pump. The D.O. peak is clearly visible in both fermentation curves (Fig. 8). The fermentations were performed at 30 °C with 500 rpm stirring and 300 L/h aeration (1.7 vvm). The minimum allowed dissolved oxygen concentration was set to 30 % and controlled by increasing stirrer speed and aeration with a cascade control on demand. Induction with a final IPTG concentration of 1 mM in the vessel was automatically initiated 4 h after the start of the feed phase. The fermentations differed from each other in terms of final cell density and protein yield. The duration of the batch phase of Nb fermentation was 13 h followed by 8 h feed phase with a final measured OD600-value of 69 (Fig. 8A). In contrast, the batch phase of Nb3K was 17 h followed by a 12 h feed phase with a final measured OD600-value of 15 (Fig. 8B).

In the higher cell density Nb fermentation, culturing was continued for 4 h post induction and cell suspension collected from the reactor with a total volume of 3.9 L. The GFP trace signal had already plateaued by the harvest time point. Nb was extracted separately from the cell pellet and the medium supertnatant as the medium supernatant was green by visual inspection. The proteins in the medium were precipitated with increasing concentrations of $(NH_4)_2SO_4$ (to final 51 %, 57 % and 70 % saturation, respectively). The pellets from precipitation were dissolved in PBS with 10 mM imidazole and purified with NiNTA.

The cell pellet was resuspended in a lysis buffer containing lysozyme, followed by three freeze-thaw cycles. After cell lysis and centrifugation, the cleared lysate was directly subjected to precipitation at 80 % $(NH_4)_2SO_4$ saturation. This saturation level was selected based on results from a prior experiment, which showed that pelleting at 70 % saturation still yielded 27.4 mg of nanobody (Table 1). The pelleted precipitate was resuspended in PBS with 10 mM imidazole and purified with sequential NiNTA and SEC chromatographies. A total of 115.6 mg pure nanobody was recovered from the medium constituting 41 % of all purified protein and 279.8 mg (59 %) from the cell pellets. Due to the high expression level of Nb and a limited capacity of the NiNTA column at hand (5 ml), the cell sample was purified by loading the NiNTA flow-through back on re-equilibriated NiNTA column for a total of three runs. Clearly, single run on 5 ml NiNTA column was not enough to sequester all Nb from the sample as only 60 % of the available Nb was captured in the first NiNTA chromatography step (Table 1). The SDS PAGE analysis of the purification is in the supplementary information (Fig. S9).

In the lower cell density Nb3K fermentation, the utility of the GFP sensor was studied in greater detail by harvesting half of the cells when the slope of the cumulative GFP trace signal started to decrease (24 h)

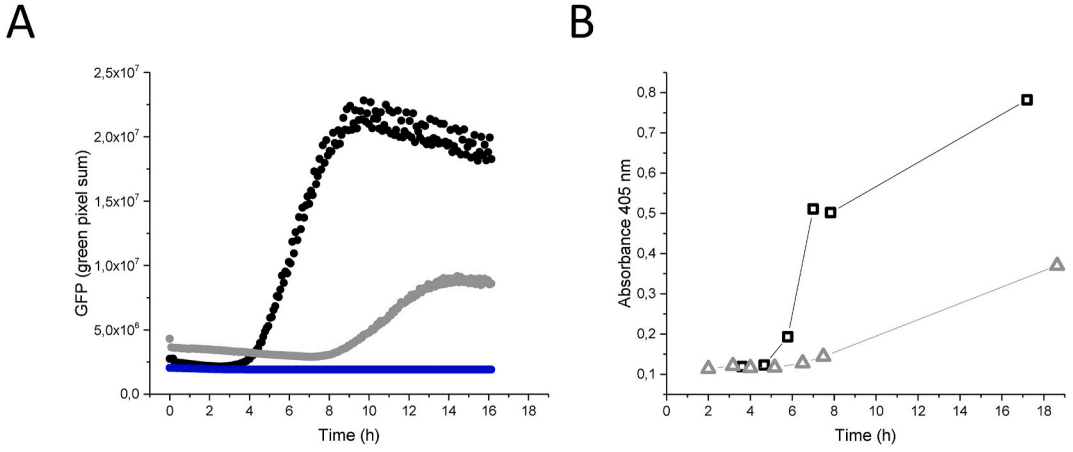

Fig. 7. Batch fermentation of Fab-AP clone CR3009 with parallel GFP promoter. A) GFP signal of induced and non-induced constructs recorded with GFP sensor. B) Fab-AP expression in induced and non-induced state as analysed by phosphatase assay using pNpp substrate. Parallel promoter construct was either induced with 400 μM IPTG at OD600 0.8 (black filled circles; black squares) or non-induced (grey filled circles; grey triangles). Original Fab-AP expression construct without parallel Lac P/O GFP cassette was used as control (blue circles). (For interpretation of the references to color in this figure legend, the reader is referred to the Web version of this article.)

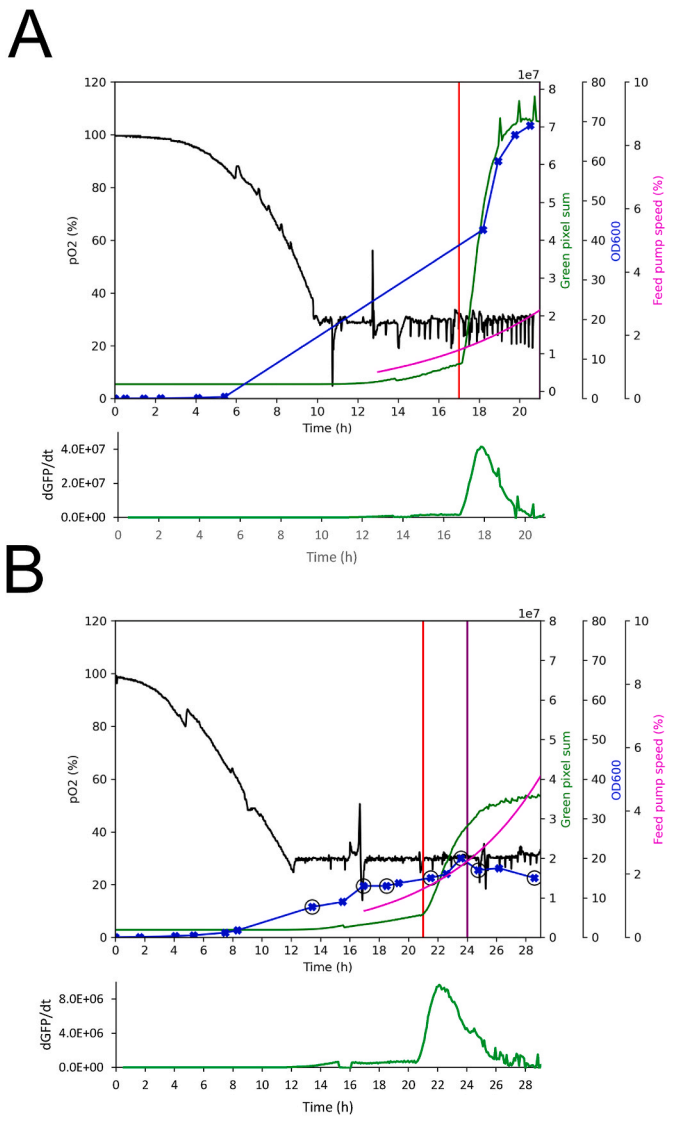

Fig. 8. Process data of nanobody fed-batch fermentations. A) Fed-batch of Nb. B) Fed-batch of Nb3K. Trace data of dissolved oxygen (pO2 (%), in-situ sensor), GFP signal from custom sensor (green pixel sum, online sensor), cell density (OD600, offline measurement) and feed profile (Feed pump speed (%), from pre-designed profile) are plotted on the graph. Red vertical line: IPTG induction; purple vertical line: first harvest (for Nb3K after 24 h incubation). The derivate (dGFP/dt) of GFP fluorescence is plotted under the respective curve. Final harvesting of cells for protein purification was executed at the end of the fermentations, which was 21 h for Nb (complete harvest) and 29 h for Nb3K (the remaining half of cells). (For interpretation of the references to color in this figure legend, the reader is referred to the Web version of this article.)

and the rest of the cells after the GFP trace signal had plateaued 5 h later. In this experiment the first harvest time was 3 h post induction. The release of Nb3K to medium was probed by western blotting cell and medium supernatant samples. At the first harvest time point there is some Nb3K visible in the medium samples (24 h) whereas at the second harvest time point (29 h) the share of released Nb3K is significantly larger (Fig. 9). The result was confirmed with an immunoassay using human IgG for capture and anti-Histag antibody-HRP for detection of the anti-human CH1 nanobody, only 0.2 % and 0.4 % of the Nb3K had leaked into the medium at 24 h and 29 h time points, respectively.

Due to the low leakage of Nb3K to the medium, Nb3K was extracted only from cells. As the yield of Nb3K cells was much lower than the yield of Nb cells, Nb3K cells were lysed directly in 200 ml of PBS +10 mM imidazole and purified from the cleared cell lysate with sequential NiNTA and SEC chromatographies without initial $(NH_4)_2SO_4$ precipitation. The flow-through (FT) from NiNTA chromatography was reloaded on re-equilibriated NiNTA column to assess if NiNTA resin binding capacity was exceeded as in earlier experiment. The 5 ml NiNTA resin bed binding capacity was adequate as 30.2, 2.52 and 0.42 mg Nb3K were recovered from the sequentially performed NiNTA-SEC chromatographies. The purification process was repeated at the end of the fermentation (29 h) for the rest of the cells with 9 % higher yield (Table 2). Size-exclusion chromatography showed two prominent peaks (Fig. S10) of which only the second eluted peak at 210 ml contained nanobody (Fig. S11).

4. Discussion

4.1. Dual promoter construct and GFP sensor station

In this study, dual GFP expression plasmid was constructed and characterized for monitoring lac promoter activation in laboratory-scale fermentation process for recombinant antibody production. The process was followed with a GFP fluorescence measurement unit placed outside the main vessel for universal applicability to various types of

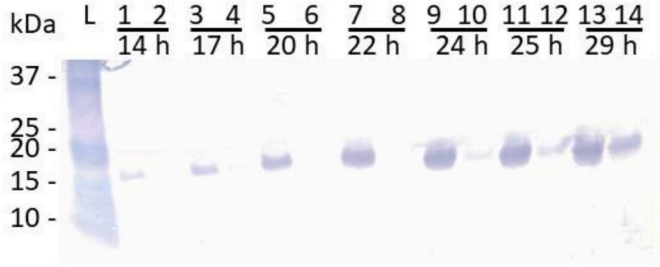

Fig. 9. Time course analysis of Nb3K leakage into medium by western blotting. Resuspended cell pellet samples (odd numbers) and medium samples (even numbers) were probed with HRP-conjugated anti-Histag antibody and precipitating TMB. Pellet samples were diluted 1/5 in H_2O before loading. L = Protein standard. Sampling time points are indicated under the lane numbers rounded to the closest full hour.

Table 1
Purification summary of Nb from cells and medium after fed-batch fermentation.

Source	Input	$(NH_4)_2SO_4$ Precipitation	Chromatography	Total (mg)
Medium	Medium	51 %	NiNTA-SEC	45.18
	Supernatant after precipitation at 51 %	57 %	NiNTA-SEC	43.00
	Supernatant after precipitation at 57 %	70 %	NiNTA-SEC	27.40
Total from medium				115.58 (41 %)
Cells	Cell lysate	80 %	NiNTA-SEC 1	168.64
	FT from NiNTA 1	–	NiNTA-SEC 2	96.72
	FT from NiNTA 2	–	NiNTA-SEC 3	14.40
Total from cells				279.76 (59 %)
Total				395.34 (100 %)

Table 2
Purification summary of Nb3K from cells collected at two harvest time points.

Source	Input	Chromatography	1/2[a] Total (mg)	2/2[b] Total (mg)	Total (mg)
Cells[c]	Cell lysate	NiNTA-SEC 1	30.16	35.0	
	FT from NiNTA 1	NiNTA-SEC 2	2.52	1.1	
	FT from NiNTA 2	NiNTA-SEC 3	0.42	0.4	
Yield			33.1	36.38	69.48
Theoretical max yield			66.2	72.76 (+9.9 %)[d]	

a) "1/2" refers to harvesting half of the cells after 24 h fermention.
b) "2/2" refers to harvesting the rest of the cells after 29 h fermention.
c) Nb 3K was purified only from cells as according to immunoassay results only 0.2 % and 0.4 % of Nb had leaked into the medium at the 1st and 2nd harvest point, respectively.
d) Yield and share of if all cells were harvested at the 1st or the 2nd time point.

bioreactors. For example, we used the designed GFP station to monitor shake-flask cultures, as it can be operated independently with the designed autoclavable feed line and a free-standing peristaltic pump. However, experiments should be designed to avoid entry of air bubbles, since the optical detection is sensitive to changes in refractive index.

Based on our investigation, orienting LacP/O-GFP cassette in identical direction as the LacP/O cassette of the gene of interest improves target protein expression. Furthermore, the simultaneous expression of GFP did not lower the expression yield of the target protein and the GFP fluorescence correlated significantly with the produced Fab-AP amount. The observation that simultaneous GFP expression with a recombinant antibody did not reduce antibody yield is interesting. This may indicate that nutrients in the complex medium were not depleted during the expression. In general, however, protein co-expression is a popular stategy in bioengineering as it has been demonstrated that simultaneous expression of chaperones can lead to higher yield of functional soluble target proteins [34]. We also confirmed that GFP fluorescence reading was not influenced by cell density neither by analysis with plate reader (Fig. 3) nor with GFP sensor station (Fig. 7).

4.2. Harvest time point

We observed that the rate of GFP fluorescence increase is a practical parameter for assessing the optimal cell harvest time if the expressed protein is to be purified from the cells. The declining rate of dGFP/dt in the fermentation experiments indicated that majority of the antibody had already been expressed. Further incubation resulted in only a minor increase in protein yield and also led to increased cell lysis. Maturation of GFP to become fluorescent causes delay between the factual expression and the detectable signal. According to literature, the maturation time t_{90} (time point when 90 % of the GFP molecules are fluorescent) of the most closely related GFP variant to this study has been reported to be 63 min at 32 °C [35]. Western blotting analysis of Nb3K fermentation samples indicated that maximal intracellular Nb3K expression had been reached in 22–24 h (Fig. 7), which is earlier than the plateau point of GFP fluorescence. Based on GFP trace data >90 % of fluorescence was obtained in Nb3K fermentation after 25 h of cultivation (Fig. 8B). The observed time gap is coherent with the known maturation time of GFP. The practical implication of the maturation delay is to terminate fermentation at least 1 h before the GFP signal plateau point is reached.

As GFP fluorescence measurement was automated with the developed online GFP sensor system, the method could be designed further to operate in a closed-loop mode, terminating the fermentation once a predetermined set point value for the decreasing dGFP/dt slope had been reached. Notably, the composition of the growth media can influence the measured pixel sum value and the dynamic range of GFP detection. Therefore, the developed GFP sensor performs optimally when used to compare experiments conducted in similar media and to monitor relative changes in GFP signal over time.

4.3. Monitoring batch and fed-batch experiments with GFP sensor

Recombinant protein production from a DNA construct may cause a significant metabolic burden on host cells [36,37]. This effect was evident in this study as Nb fed-batch fermentation resulted in approximately five times higher cell and protein titers compared to Nb3K fermentation. Concomitantly, GFP co-expression analysis showed that Nb production was finished 6 h earlier than Nb3K production. Nb3K biomass accumulation was not coherent to the precalculated fed-batch model after 24 h incubation, which most likely resulted in excess glucose being accumulated in the reactor, which may have affected the protein production yield in the final hours by catabolite repression mechanism. As the GFP sensor data serves as a proxy for the expression rate and yield of the target protein, this technology could be a useful tool for both optimizing the space–time yield of a process and supporting clonal selection in strain engineering, for which another dual reporter promoter system has also been recently established [38]. The observed problems with Nb3K production could possibly be overcome by changing the expression host strain and even host to eukaryotic species with the added benefit of functional post-translational modification machineries [39].

Besides informing on the stage of fermentation process, GFP sensor can be used to monitor induction success. In Fab-AP CR3009 batch fermentation experiments clear differences were observed in GFP fluorescence accumulation and antibody expression between the induced and non-induced batches. Early identification of failed production batches minimizes unnecessary analytical and purification efforts later in the process. According to our experience, the introduction of GFP sensor with dual GFP promoter expression is especially useful tool for bioprocess education as it visually demonstrates promoter induction for students in real time. It provides a unique process parameter for evaluating expression success, e.g., under optimal IPTG induction versus catabolite repression, and it also serves as an indicator of successful cell lysis in downstream processing. Overall, tracking Lac P/O promoter activation with GFP dual promoter construct is a valuable addition to the conventional process data parameters. Finally, as this study demonstrates, low-cost and accessible technologies such as 3D printing, single-board computers, and open-source code enable the implementation of novel process analytical tools and showcase the potential for innovation in bioprocess engineering despite funding constraints.

CRediT authorship contribution statement

Anttoni Korkiakoski: Writing – original draft, Visualization, Software, Methodology, Investigation, Formal analysis, Data curation. **Sami Oksanen:** Writing – review & editing, Investigation. **Tuomas Huovinen:** Writing – review & editing, Writing – original draft, Visualization, Validation, Supervision, Investigation, Formal analysis, Conceptualization.

Statements and declarations

Authors declare no competing interests.

Funding

This research did not receive any specific grant from funding agencies in the public, commercial, or not-for-profit sectors.

Acknowledgements

We thank Prof. Tero Soukka for helpful discussions and the undergraduate students of the Department of Life Technologies for generating data from numerous experiments with the GFP sensor station, which have been of utmost importance for the further development of the concept.

Appendix A. Supplementary data

Supplementary data to this article can be found online at https://doi.org/10.1016/j.pep.2025.106808.

Data availability

Data will be made available on request.

References

[1] R. Fu, L. Carroll, G. Yahioglu, E.O. Aboagye, P.W. Miller, Antibody fragment and affibody ImmunoPET imaging agents: radiolabelling strategies and applications, ChemMedChem 13 (2018) 2466–2478, https://doi.org/10.1002/CMDC.201800624.
[2] A. Bates, C.A. Power, David vs Goliath, The structure, function, and clinical prospects of antibody fragments, Antibodies 8 (2019) 28, https://doi.org/10.3390/antib8020028.
[3] O. Spadiut, S. Capone, F. Krainer, A. Glieder, C. Herwig, Microbials for the production of monoclonal antibodies and antibody fragments, Trends Biotechnol. 32 (2014) 54–60, https://doi.org/10.1016/J.TIBTECH.2013.10.002.
[4] A. Sarker, A.S. Rathore, R.D. Gupta, Evaluation of scFv protein recovery from E. coli by in vitro refolding and mild solubilization process, Microb. Cell Fact. 18 (2019), https://doi.org/10.1186/S12934-019-1053-9.
[5] A. Frenzel, M. Hust, T. Schirrmann, Expression of recombinant antibodies, Front. Immunol. 4 (2013), https://doi.org/10.3389/FIMMU.2013.00217.
[6] T. Shibui, K. Nagahari, Secretion of a functional fab fragment in Escherichia coli and the influence of culture conditions, Appl. Microbiol. Biotechnol. 37 (1992) 352–357, https://doi.org/10.1007/BF00210991.
[7] A. Plückthun, A. Skerra, Expression of functional antibody Fv and fab fragments in Escherichia coli, Methods Enzymol. 178 (1989) 497–515, https://doi.org/10.1016/0076-6879(89)78036-8.
[8] A.L. Demain, P. Vaishnav, Production of recombinant proteins by microbes and higher organisms, Biotechnol. Adv. 27 (2009) 297–306, https://doi.org/10.1016/j.biotechadv.2009.01.008.
[9] P.T. Wingfield, Overview of the purification of recombinant proteins, Curr. Protoc. Protein Sci. 80 (6.1.1–6.1.35) (2015), https://doi.org/10.1002/0471140864.PS0601S80.
[10] L. Randers-Eichhorn, C.R. Albano, J. Sipior, W.E. Bentley, G. Rao, On-Line green fluorescent protein sensor with LED excitation, John Wiley & Sons, Inc. Biotechnol. Bioeng. 55 (1997) 921–926, https://doi.org/10.1002/(SICI)1097-0290(19970920)55:6.
[11] O. Shimomura, F.H. Johnson, Y. Saiga, Extraction, purification and properties of aequorin, a bioluminescent protein from the luminous hydromedusan, aequorea, J. Cell. Comp. Physiol. 59 (1962) 223–239, https://doi.org/10.1002/JCP.1030590302.
[12] E.A. Rodriguez, R.E. Campbell, J.Y. Lin, M.Z. Lin, A. Miyawaki, A.E. Palmer, X. Shu, J. Zhang, R.Y. Tsien, The growing and glowing toolbox of fluorescent and photoactive proteins, Trends Biochem. Sci. 42 (2017) 111–129, https://doi.org/10.1016/J.TIBS.2016.09.010.
[13] W.W. Su, Fluorescent proteins as tools to aid protein production, Microb. Cell Fact. 4 (2005), https://doi.org/10.1186/1475-2859-4-12.
[14] J.J. Jones, A.M. Bridges, A.P. Fosberry, S. Gardner, R.R. Lowers, R.R. Newby, P. J. James, R.M. Hall, O. Jenkins, Potential of real-time measurement of GFP-fusion proteins, J. Biotechnol. 109 (2004) 201–211, https://doi.org/10.1016/j.jbiotec.2003.10.039.
[15] H.J. Cha, N.G. Dalal, M.-Q. Pham, V.N. Vakharia, G. Rao, W.E. Bentley, Insect larval expression process is optimized by generating fusions with green Fluorescent protein, Biotechnol. Bioeng. 65 (1999) 316–324, https://doi.org/10.1002/(SICI)1097-0290(19991105)65:3.
[16] D.E. Drew, G. Von Heijne, P. Nordlund, J.W.L. De Gier, Green fluorescent protein as an indicator to monitor membrane protein overexpression in Escherichia coli, FEBS Lett. 507 (2001) 220–224, https://doi.org/10.1016/S0014-5793(01)02980-5.
[17] B.J. Feilmeier, G. Iseminger, D. Schroeder, H. Webber, G.J. Phillips, Green fluorescent protein functions as a reporter for protein localization in Escherichia coli, J. Bacteriol. 182 (2000) 4068–4076, https://doi.org/10.1128/JB.182.14.4068-4076.2000.
[18] S.S. Daabrowski, A. Brillowska, J. Kur, Use of the green fluorescent protein variant (YFP) to monitor MetArg human proinsulin production in Escherichia coli, Protein Expr. Purif. 16 (1999) 315–323, https://doi.org/10.1006/PREP.1999.1072.
[19] S.I. Tan, S.C. You, I.T. Shih, I.S. Ng, Quantification, regulation and production of 5-aminolevulinic acid by green fluorescent protein in recombinant Escherichia coli, J. Biosci. Bioeng. 129 (2020) 387–394, https://doi.org/10.1016/J.JBIOSC.2019.10.005.
[20] M.P. Delisa, J. Li, G. Rao, W.A. Weigand, W.E. Bentley, Monitoring GFP-operon fusion protein expression during high cell density cultivation of Escherichia coli using an On-line optical sensor, Biotechnol. Bioeng. 65 (1999) 54–64, https://doi.org/10.1002/(SICI)1097-0290(19991005)65:1.
[21] Y. Kostov, C.R. Albano, G. Rao, COMMUNICATION TO THE EDITOR all solid-state GFP sensor, Sons, Inc. Biotechnol. Bioeng. 70 (2000) 473–477, https://doi.org/10.1002/1097-0290(20001120)70:4.
[22] H. Zhu, O. Yaglidere, T.W. Su, D. Tseng, A. Ozcan, Cost-effective and compact wide-field fluorescent imaging on a cell-phone, Lab Chip 11 (2011) 315–322, https://doi.org/10.1039/C0LC00358A.
[23] M. Hattori, S. Shirane, T. Matsuda, K. Nagayama, T. Nagai, Smartphone-based portable bioluminescence imaging system enabling observation at various scales from whole mouse body to organelle, Sensors (Basel) 20 (2020) 1–12, https://doi.org/10.3390/S20247166.
[24] L.M. Aufdembrink, P. Khan, N.J. Gaut, K.P. Adamala, A.E. Engelhart, Highly specific, multiplexed isothermal pathogen detection with fluorescent aptamer readout, RNA 26 (2020) 1283–1290, https://doi.org/10.1261/RNA.075192.120/-/DC1.
[25] J.W. Jolles, Broad-scale applications of the raspberry Pi: a review and guide for biologists, Methods Ecol. Evol. 12 (2021) 1562–1579, https://doi.org/10.1111/2041-210X.13652.
[26] E.N. van den Brink, J. ter Meulen, F. Cox, M.A.C. Jongeneelen, A. Thijsse, M. Throsby, W.E. Marissen, P.M.L. Rood, A.B.H. Bakker, H.R. Gelderblom, B. E. Martina, A.D.M.E. Osterhaus, W. Preiser, H.W. Doerr, J. de Kruif, J. Goudsmit, Molecular and biological characterization of human monoclonal antibodies binding to the spike and nucleocapsid proteins of severe acute respiratory syndrome coronavirus, J. Virol. 79 (2005) 1635–1644, https://doi.org/10.1128/JVI.79.3.1635-1644.2005.
[27] T. Huovinen, M. Syrjänpää, H. Sanmark, E.C. Brockmann, A. Azhayev, Q. Wang, M. Vehniäinen, U. Lamminmäki, Two ScFv antibody libraries derived from identical VL-VH framework with different binding site designs display distinct binding profiles, Protein Eng. Des. Sel. 26 (2013) 683–693, https://doi.org/10.1093/PROTEIN/GZT037.
[28] R. Kilgard, A.B. Heim, R.Y. Tsien, Improved green fluorescence, Nature 373 (1995) 663–664, https://doi.org/10.1038/373663B0.
[29] O. Scholz, A. Thiel, W. Hillen, M. Niederweis, Quantitative analysis of gene expression with an improved green fluorescent protein, Eur. J. Biochem. 267 (2000) 1565–1570, https://doi.org/10.1046/J.1432-1327.2000.01170.X.
[30] G.S. Waldo, B.M. Standish, J. Berendzen, T.C. Terwilliger, Rapid protein-folding assay using green fluorescent protein, Nat. Biotechnol. 17 (1999) 691–695, https://doi.org/10.1038/10904.
[31] W.J.J. Hermans, S. Blokland, M.A. van Kesteren, J.M. Horrevoets, F.J.M. Detmers, Antigen-binding protein directed against epitope in the CH1 domain of human IgG antibodies. European Patent EP2670779B1, European Patent Office, 2013.
[32] A. Krebber, S. Bornhauser, J. Burmester, A. Honegger, J. Willuda, H.R. Bosshard, A. Plückthun, Reliable cloning of functional antibody variable domains from hybridomas and spleen cell repertoires employing a reengineered phage display system, J. Immunol. Methods 201 (1997) 35–55, https://doi.org/10.1016/S0022-1759(96)00208-6.
[33] F. Jacob, J. Monod, Genetic regulatory mechanisms in the synthesis of proteins, J. Mol. Biol. 3 (1961) 318–356, https://doi.org/10.1016/S0022-2836(61)80072-7.
[34] D.M. Francis, R. Page, Strategies to optimize protein expression in E. coli, Curr. Protoc. Protein Sci. Chapter 5 (2010), https://doi.org/10.1002/0471140864.PS0524S61.
[35] E. Balleza, J.M. Kim, P. Cluzel, Systematic characterization of maturation time of fluorescent proteins in living cells, Nat. Methods 15 (2018) 47–51, https://doi.org/10.1038/NMETH.4509.
[36] Z. Li, U. Rinas, Recombinant protein production associated growth inhibition results mainly from transcription and not from translation, Microb. Cell Fact. 19 (2020), https://doi.org/10.1186/S12934-020-01343-Y.
[37] W.E. Bentley, N. Mirjalili, D.C. Andersen, R.H. Davis, D.S. Kompala, Plasmid-encoded protein: the principal factor in the "metabolic burden" associated with recombinant bacteria, Biotechnol. Bioeng. 35 (1990) 668–681, https://doi.org/10.1002/BIT.260350704.
[38] A. Zutz, L. Hamborg, L.E. Pedersen, M.M. Kassem, E. Papaleo, A. Koza, M. J. Herrgård, S.I. Jensen, K. Teilum, K. Lindorff-Larsen, A.T. Nielsen, A dual-reporter system for investigating and optimizing protein translation and folding in E. coli, Nat. Commun. 12 (2021), https://doi.org/10.1038/S41467-021-26337-1.
[39] A. Schütz, F. Bernhard, N. Berrow, J.F. Buyel, F. Ferreira-da-Silva, J. Haustraete, J. van den Heuvel, J.E. Hoffmann, A. de Marco, Y. Peleg, S. Suppmann, T. Unger, M. Vanhoucke, S. Witt, K. Remans, A concise guide to choosing suitable gene expression systems for recombinant protein production, STAR Protoc. 4 (2023), https://doi.org/10.1016/j.xpro.2023.102572.